LIMPACT: A Hydraulically Powered Self-Aligning Upper Limb Exoskeleton

Alexander Otten, Carsten Voort, Arno Stienen, Ronald Aarts, Edwin van Asseldonk, and Herman van der Kooij

***Abstract*—The LIMPACT is an exoskeleton developed to be used in identifying the reflex properties of the arm in stroke survivors. Information on joint reflexes helps in designing optimal patient specific therapy programs. The LIMPACT is dynamically transparent by combining a lightweight skeleton with high power to weight ratio actuators. The LIMPACT is supported by a passive weight balancing mechanism to compensate for the weight of the exoskeleton and the human arm. Various self-aligning mechanisms allow the human joint axes to align with the axes of the exoskeleton which ensure safety and short don/doff times. The torque-controlled motors have a maximum torque bandwidth of 97 Hz which is required for fast torque perturbations and smooth zero impedance control. The LIMPACT's weight is reduced five times as gravitational forces are lowered using a model-based gravity compensation algorithm. The impedance controller ensures tracking of a cycloidal joint angle reference. A cycloid with an amplitude of 1.3 rd and a maximum velocity of 6.5 rd/s has a maximum tracking error of only 7%. The LIMPACT fulfills the requirements to be used in future diagnostics measurements for stroke patients.**

***Index Terms*—Compensation, hydraulic systems, modeling, predictive control, robots.**

I. Introduction

EACH year, approximately 15 million people worldwide have a stroke. Of these stroke victims, 23% are permanently disabled and will experience problems with arm movements [1]. Common problems are muscle synergies, spasticity, lack of joint control and weakness. Intense physical therapy can help regain some of the normal functional arm movements. For an optimal and efficient therapy program, more insight is needed in the pathophysiological processes underlying the motor impairments such that interventions can be designed that specifically address these disturbed pathophysiological processes. The importance of these different pathophysiological processes in explaining the movement impairments differs widely between patients. To tailor therapy to individual needs, the first step is to identify these contributions. However, current approaches to quantify these processes are mainly performed in static situations, which do not necessarily tell us how these processes influence movement. Especially quantifying the importance of disturbed reflexes is a big challenge.

The dynamic properties of the arm are governed by the inertia and mass of the arm and damping and stiffness resulting from intrinsic (i.e., muscular) and reflexive properties. Joint reflexes and stiffness give information about motor impairments which helps in designing support strategies in therapy programs. Reflexive dynamic properties can be separated from the intrinsic dynamic properties by first determining the latter. The intrinsic joint dynamics can then be subtracted from a combined dynamic response to reveal the dynamics of the reflex pathway [2]. This requires application of a position [2], [3], velocity [4] or torque [5] perturbation and measurement of the resulting torque or position dynamic response. The required perturbations should have speeds of 5 rd/s and up [4] or a minimum (force) frequency content of 20 Hz [5], [6]. Robots can be used to apply the perturbation and to measure the response.

Exoskeletons (see Fig. 1) are a special type of robotic devices. They are attached to the arm of a human and are designed to be dynamically transparent, comfortable, safe and should align with the human axes. They are able to apply torques for assistance or perturbation and to measure torque or position responses.

Many exoskeletons are available or under development. They are used in teleoperation [7], as human force amplifiers [8], [9], as haptic devices [10], [11] and for training and diagnostics in rehabilitation of stroke patients [12]–[29]. The only commercially available rehabilitation exoskeleton for stroke patients is the ArmeoPower (based on the ARMin III [12]). However, none of them are suitable for applying fast multijoint perturbations to a human arm. The perturbations combined with the dynamics of the exoskeleton and human arm require a high powered, fast and accurately measuring exoskeleton. Current state of the art exoskeletons are either light and low torque [16], [18], [23], [27], [29] or are relatively heavy, high torque and slow moving devices [10], [12], [14], [15], [20].

Other diagnostic robotic devices are limited to one [3]–[5], [30], [31] or two degrees of freedom (DOFs) [2], [6], [32]. The main issue of these devices is that they cannot be used to detect multijoint reflex impairments [6] which is an indication of the level of the motor impairment following stroke [33].

Manuscript received December 10, 2013; revised September 24, 2014; accepted November 6, 2014. Date of publication February 18, 2015; date of current version August 24, 2015. Recommended by Technical Editor O. Kaynak. This work was supported in part by SenterNovem and Provincie Overijsel, The Netherlands, under Grant Pieken in de Delta—Oost Nederland, Project VirtuRob and Grant 1-5160.

A. Otten, C. Voort, and E. van Asseldonk are with the Laboratory of Biomechanical Engineering, University of Twente, 7522 Enschede, The Netherlands (e-mail: a.otten@utwente.nl; h.c.voort@utwente.nl; e.h.f.vanasseldonk@utwente.nl).

A. Stienen is with the Laboratory of Biomechanical Engineering, University of Twente, 7522 Enschede, The Netherlands, and also with the Neuro Imaging and Motor Control Laboratory, Northwestern University, Chicago, IL 60611 USA (e-mail: arnostienen@gmail.com).

R. Aarts is with the Laboratory of Mechanical Automation, University of Twente, 7522 Enschede, The Netherlands (e-mail: r.g.k.m.aarts@utwente.nl).

H. van der Kooij is with the Laboratory of Biomechanical Engineering, University of Twente, 7522 Enschede, The Netherlands, and also with the BioMechanical Engineering Group, University of Delft, Delft 2628, The Netherlands (e-mail: h.vanderkooij@tudelft.nl).

Color versions of one or more of the figures in this paper are available online at http://ieeexplore.ieee.org.

Digital Object Identifier 10.1109/TMECH.2014.2375272

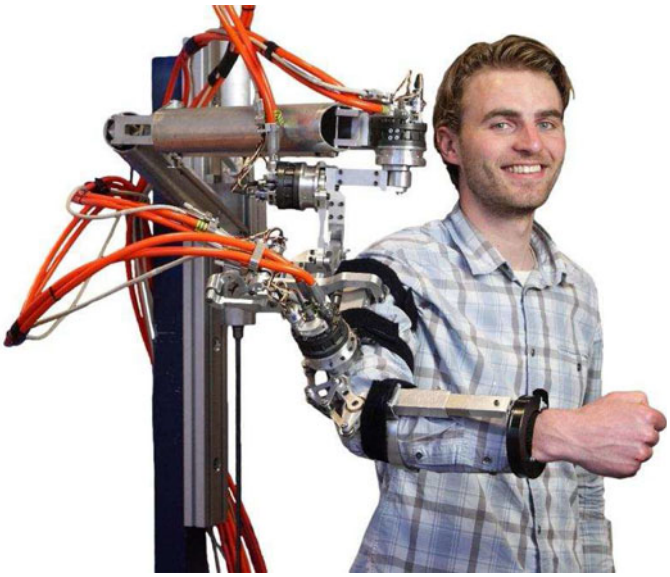

Fig. 1. LIMPACT: a hydraulically powered exoskeleton for the upper extremity. A passive weight support linkage is connected to the blue base frame which supports the exoskeleton and enables the base of the exoskeleton to translate but not rotate. Four gray hydraulic rotational motors are connected with orange hoses to the hydraulic pump unit (not shown). Note that the safety covers have been removed for a clearer view of the exoskeleton itself.

Apart from the need to design a lightweight but powerful exoskeleton, there is a need to design exoskeletons that assure a proper alignment of the exoskeleton and human arm. This is crucial not only for comfort, but also for safety. Misalignment of the joints can cause severe pain especially when high torques are involved. Since alignment of the axes is challenging to do visually, self-aligning of the shoulder [34] and elbow joints [35] is an ideal way to solve the problem of manual aligning. Next to that, self-aligning mechanisms also reduce do on/do off (don/doff) times.

The goal is to develop an exoskeleton that can perform diagnostic measurements on stroke survivors to gain knowledge for optimizing rehabilitation therapies. Based on its predecessor the Dampace [36], [37], we aimed to design and build an exoskeleton that combines a lightweight skeleton with powerful motors, has a short don/doff time, is dynamically transparent and safe. We designed the LIMPACT which will presented in this paper.

Various design choices were made in the mechanical, actuation and control design to meet the specifications required for an exoskeleton that can be used in diagnostic measurements. Details of the specifications and the design are described in Section II. The modeling structure is depicted in Section III. The development of the controller is described in Section IV and the simulation and experimental results are shown in Section V. Section VI contains a detailed discussion.

II. Design

A. Requirements

A human arm has three rotational (ab/adduction, flex/extension and in/external rotation) and two translational (elevation/depression and re/protraction) DOFs in the shoulder, two DOFs in the elbow (flex/extension and pro/supination) and two in the wrist (flex/extension and ulnar/radial deviation). When designing an exoskeleton, the ROM of the exoskeleton should not overly confine the human ROM, but, for safety reasons, should not exceed it as well.

TABLE I
Design Targets and Achieved Values

Property	Target	Achieved
Sh. Abd./Add. [deg]	100	120
Sh. Int./Ext. Rot. [deg]	135	120
Sh. Flex./Ext. [deg]	110	120
El. Flex./Ext. [deg]	150	135
El. Sup./Pro. [deg]	150	180
Range X shoulder alignment [mm]	200	250
Range Y shoulder alignment [mm]	200	250
Range Z shoulder alignment [mm]	300	350
Range elbow alignment [mm]	50	70
Upper arm lengths [mm]	253–442	261–338
Lower arm lengths [mm]	98–260	177–261
Maximum motor torque [Nm]	20	36
Motor torque bandwidth [Hz]	40	43–102
Controlled motor power [kW]	0.25	0.3–3.2
Stiffness elastic element [Nm/rd]	200	170–180

The achievable position bandwidth of the human arm is in the order of 2–5 Hz [38], [39]. The (torque) control bandwidth is approximately 7 Hz [38]. Torques of up to 10 Nm are required in activities of daily living (ADL) [15], [40]. Additional torques are needed for moving the exoskeleton itself. The identification of the reflex properties of the arm requires movement perturbations up to 20 Hz [5], [6].

The exoskeleton is designed using the anthropometry data for male and female Dutch adults (31–60 years). This group (5–95%) has an upper arm length (mean $\pm$ standard deviation) in the range of 346 ± 96 mm and a lower arm in the range of 179 ± 81 mm [41]. The exoskeleton should be adjustable to these various arm lengths and sizes.

The design targets are shown in Table I in descending order: 1) ROM of the joints, 2) range of the alignment mechanisms, 3) adjustability and 4) motor performance. 1) The ROM of the joints follows from the ROM of the human arm. 2) The range of the shoulder alignment mechanism is determined by the various *xyz*-dimensions. The elbow alignment range is revered to be as large as possible for the lowest don/doff times (see Section II-D). 3) The arm length variations are defined by the selected patient group. 4) The motor specifications are derived from by the required perturbations it has to deliver to the human arm.

B. Linkage

The LIMPACT setup is shown in Fig. 2 and can be divided into four subassemblies, i.e., the support linkage, its skeleton, the elbow alignment mechanism and the motor design. First, the support linkage will be discussed.

The support linkage (see Figs. 3 and 4) acts as a passive support mechanism to support the exoskeleton's weight such

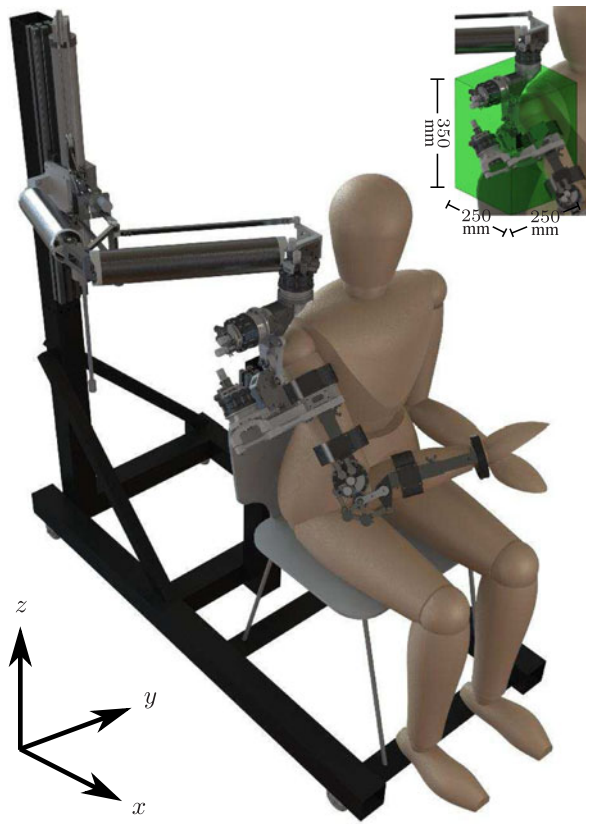

Fig. 2. Rendering of the complete device including frame, support linkage, exoskeleton, chair and subject. Note that the hoses are not drawn here for a clearer view of the components.

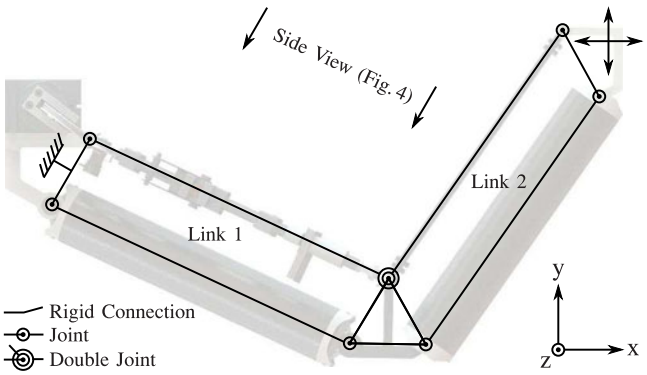

Fig. 3. Schematic top view of the linkage weight support mechanism. From the top, the linkage mechanism consist of two parallelogram linkages enabling two translational DOF in the x- and y-direction at the endpoint.

that the weight of the exoskeleton is not lifted by the patient. The support mechanism can also partially or fully support the weight of the arm of the patient. Next to supporting the weight, the linkage also ensures self-alignment of the human shoulder and the exoskeleton. The support mechanism is derived from [42] and more information on the design can be found in [43].

A side view of the support mechanism is shown in Fig. 4 where one of the parallel linkages is shown. The linkage can move in the z-direction and is supported by the spring force

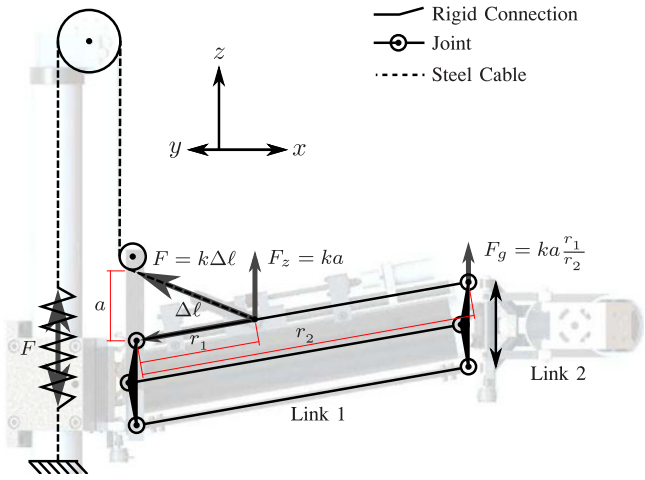

Fig. 4. Schematic side view of the linkage weight support mechanism. The linkage mechanism consists of one parallelogram linkage enabling one translational DOF in the z-direction at the endpoint. A pretensioned zero-length spring with force F creates a gravitation compensation force F_g which can be changed by altering r_1, the position of F_z along link 1 using an electric motor. The force F_g is only dependent on dimensions a, r_1, r_2 and stiffness k.

TABLE II
PROPERTIES OF SUPPORT LINKAGE

Name	Symbol	Value	Unit
Dimension	r_2	400	mm
Dimension	$r_{1,\mathrm{min}}$	75	mm
Dimension	$r_{1,\mathrm{max}}$	158	mm
Dimension	a	85	mm
Stiffness	k	5.47	N/mm
Force	$F_{g,\mathrm{min}}$	87	N
Force	$F_{g,\mathrm{max}}$	184	N
Translation	x	250	mm
Translation	y	250	mm
Translation	z	350	mm

F. The zero-length spring is attached to the parallel linkage by an aramid cable. The force F_z is only dependent on the stiffness k and the dimension a and therefore remains constant at all times. A linear guidance with an electric spindle drive motor is mounted to alter the ratio $r_1:r_2$. A changing in the ratio $r_1:r_2$ will change the moment arm thus changing the gravity compensating force F_g at the endpoint. The force F_g may be placed at the endpoint of link 2 as the strictly horizontal linkage does not increase the moment arm and can guide torques back to the base frame.

The parallel linkage link 1 is equipped with universal (two DOF) joints such that the end point can move in the z-direction and rotate around the z-axis. The combination of link 1 and 2 enable the endpoint to move in the x-, y- and z-direction. The parallel linkages are build with push/pull rods which can only restrict torques in one direction. The two linkages are therefore equipped with hollow tubes that have a large torsional stiffness. The tube guides the torques that the parallel linkages cannot handle to the base frame. The specifications of the support linkage are given in Table II.

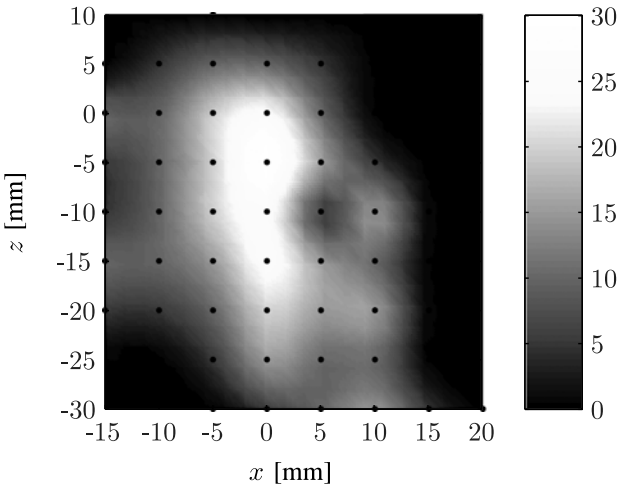

Fig. 5. Adjustability of the elbow alignment mechanism valid for elbow rotations from 5–65 °. The elbow is position in x- and z-direction (see Fig. 7) through fixating the upper arm to the exoskeleton with the origin located in the center of the elbow motor (but not necessarily the elbow axis). The surface plot shows the range at which the lower arm can be fixated to the exoskeleton such that no collisions of the mechanism occur and the elbow will have full ROM.

C. Skeleton

The LIMPACT's skeleton is built using aluminium hollow profiles to minimize weight and maximize strength (see Fig. 7). The mass of the exoskeleton is 8 kg (4 kg when the four motors are excluded) which is slightly above average compared to the reported weight of other rehabilitation exoskeletons. The exoskeleton is equipped with lightweight, custom-made carbon fiber braces combined with comfortable velcro straps. The braces can be exchanged for arm circumferences of approximately 120, 100, 80 and 60 mm. The length of the upper arm of the exoskeleton can be adjusted within a range 261–338 mm and and lower arm within 177–261 mm (see Fig. 7).

D. Elbow Alignment

The first elbow joint has a self-aligning mechanism (axis 4) which allows significant position freedom for the human elbow joint relative to the exoskeleton. The second elbow joint is passive, in line with the lower arm and enables forearm pro/supination.

The self aligning mechanism for the elbow is shown at the bottom of Fig. 7. The mechanism consists of two parallelograms (q_{11}-q_{12}-q_{15}-q_{21} and q_{13}-q_{16}-q_{22}-q_{23}) and one four-bar linkage (q_{12}-q_{14}-q_{16}-q_{23}). The human elbow joint q_{14} is part of the four-bar linkage. If the human arm is not attached to the exoskeleton, the elbow alignment mechanism is underdetermined and able to translate freely in the x- and z-direction. The motor shaft q_4 is positioned slightly behind the axis of the arm (13 mm) since the anatomic position of the elbow axis is also position slightly behind the central axis of the upper arm (10–20 mm).

To determine the allowable adjustment range of the elbow, we first need the procedure for fixing a patient's arm in the exoskeleton. This is done by firstly fixating the proximal upper brace to the patient's upper arm. The exoskeleton is adjusted to the upper arm of the subject by adjusting $q_{\ell 1}$ after which the distal upper brace is attached to the patient's upper arm. The lower arm can be strapped in by fixing the proximal forearm brace of the lower arm to the patients arm. The configuration of the alignment mechanism should be similar to Fig. 7. The exoskeleton is adjusted to the length of the lower arm by altering $q_{\ell 2}$ and the distal forearm brace can be attached to the lower arm. This procedure takes about 1 min.

The range of the self aligning mechanism is analyzed. The upper arm of the exoskeleton and patient are set as the fixed world so that the location of the elbow is determined. The remaining adjustability is the placement of the upper brace on the lower arm of the patient. The placement of the proximal forearm brace on the lower arm with respect to the location of the elbow is shown in Fig. 5 which represents the adjustability of the elbow.

E. Hydraulic Motor

The selection of the motor has a significant impact on all aspects of the design. Electric motors are most often chosen [10], [11], [14], [15], [17]–[20], [22], [28], [29], [44]. Alternatively, pneumatic [23]–[27] or hydraulic motors [9] can be used.

Electric motors are popular since they are easy to control, widely available, have a broad variety of specifications and are low in cost. However, they are usually equipped with a transmission to increase the output torque which can reduce stiffness, introduces reflective inertia, reduces backdrivability and bandwidth and may introduce play, friction and electrical disturbance that can strongly interfere with the sensor signals. The mechanical disturbances, e.g., reflective inertia, friction and stiffness can be handled using disturbance observers [45]–[47] or state feedback control [48]–[50], but they still do not have the best power to weight ratio [51].

An alternative is the pneumatic motor which is lightweight and can be fast. Its main limitations are the maximum pressure of approximately 0.8 MPa which impact the motor dimensions, its complex control algorithm needed to handle the air compressibility and flow dynamics and motor friction and the general lack of control stiffness for forced perturbations.

Hydraulic motors are rarely chosen except for in the SARCOS exoskeleton and SARCOS big arm teleoperation system. Hydraulic systems require a complex control algorithm to handle flow dynamics and motor friction. They need an expensive installation including a pump, valves, hoses and an electric motor. However, hydraulics have the best torque to weight ratio and power to weight ratio [51]. Especially the latter is required when perturbations need to be generated for diagnostic measurements.

The LIMPACT is equipped with four rotational series elastic hydraulic motors, one of them shown in Fig. 6 including its low stiffness torsion spring. The four springs minimizes play and friction, ensures a smooth torque controllability and they do not introduce reflective inertia. The low stiffnesses reduce the position control bandwidth, but increases the torque fidelity and torque measuring accuracy [52], [53]. The motor is made of hard anodized aluminium, has a weight of 1 kg and is designed for an oil pressure of 8 MPa to produce 50 Nm.

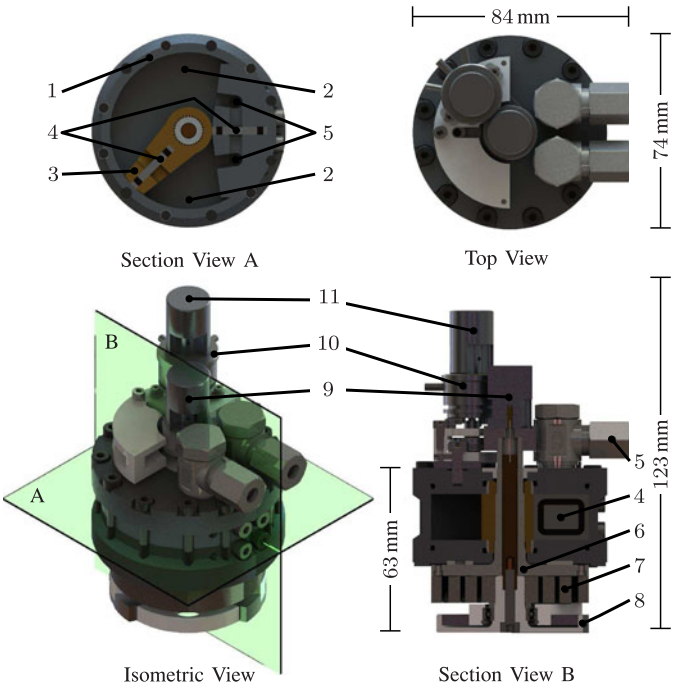

Fig. 6. Isometric and top view of the hydraulic motor as well as a horizontal (A) and vertical (B) section view. The hydraulic motor is built up with a cylinder (1) which contains two chambers (2) created by the vane (3) and the window seals (4). Oil pressure in the chambers can be regulated by an oil flow through the in- and outlet ports (5). The motor shaft (6) is connected to the elastic element (7) where the latter is connected to the joint flange (8). The defection of the elastic element is measured using an encoder (9). The motor angle is measured using a potentiometer (10) and encoder (11) in combination with a high precision pulley drive.

Note that in a series elastic motor the torque between the motor and exoskeleton is measured by measuring the spring deflection and knowing the spring stiffness. The combination of spring stiffness and spring deflection results in a torque measurement which will be used in the torque control loop. The resulting mass-spring system will filter out any high frequency vibration coming from the motor which increases comfort. Since the torque sensing is done after the motor, stick-slip friction and nonlinearities will be compensated for and a low-controlled impedance can be achieved [54].

The deflection of the torsion spring is accurately measured using a high resolution AEDA-3300 encoder (80 000 pulses per revolution, Avago Technologies, San Jose, CA, USA). The spring deflection is multiplied with the identified spring stiffness to determine the torque applied to the joint of the exoskeleton. The motor angle is measured using a FCPS22AC potentiometer (Altheris, Leidschendam, The Netherlands) and an AEDA-3300 encoder via a high precision pulley drive. The potentiometer is used to initialize the encoder and as a redundant sensor. The potentiometer is calibrated using the encoder to increase precision.

F. Safety

The safety system is built up out of three layers: the software layer, the electric layer and the mechanical layer. The first layer, the software layer, ensures safety by limiting power, limiting torque and it has a jam detection. It also has a built in software-controlled safety stop which limits the range of the exoskeleton.

The second layer, an analog electric safety layer, contains window detectors that are electrically separated from the controlled system. A (redundant) angle or force sensor is connected to which a range can be set. If the sensed signal is out of range, the analog electric safety switches the system off. The latter means that disconnected wires or short circuits are also detected. Other safety features are a power enable function which ensures only a power on when all is in order, a beacon which flashes when the system is operating and a watchdog function. Pressure sensors (UNIK 5000 - PMP 5076-TB-A1-CA-H0-PA, General Electric, Fairfield, USA) are used for torque redundancy measurement at the valve side and for guarding the supply pressure at the pump side.

The third layer is the mechanical safety system. It contains end-stops that limit the range of the LIMPACT to a range less than that of a human arm and hydraulic hose covers that protect against hose leakage and mechanical covers that prevent snipping. The hydraulic installation can be purged fast when needed and has a passive high and low power setting. The low setting is used when subjects are strapped to the exoskeleton.

III. Modeling

A. Rigid Body Model

The exoskeleton has a total of 20 revolute joints connecting 18 rigid bodies (see Fig. 7) and can be divided into four submodels. A DOF can be independent (actuated), dependent (to the actuated joint) or constrained. The latter term states that for, e.g., a revolute joint, the specified revolute DOF is released (or dependent) and the other five DOFs of the joint are constrained using springs and dampers. This method is used in solving parallel structures such as a four link mechanism.

The four submodels are shown in Fig. 7 and the first submodel can be represented as a simple-actuated joint q_1. The second submodel in Fig. 7 is a four-bar linkage with two dependent DOFs q_5 and q_6 and one constrained DOF q_{17}. The three DOFs have a one-to-one linear relation to the independent actuated DOF q_2. The actuated submodel 3 in Fig. 7 is more complex as it is composed of one independent actuated DOF q_3, three constrained DOF $q_{18\cdots20}$ and four dependent DOFs. Still, the relation between the constrained, dependent and independent DOFs is a one-to-one linear relation.

The last submodel in Fig. 7 consists of one independent actuated DOF q_4, three constrained DOFs $q_{21\cdots23}$ and three dependent DOFs. The joint is only determined when a human elbow axis is present. The relation between the dependent joints and the actuated independent DOF q_4 is nonlinear since the coordinates of the elbow joint are unknown. The constrained DOFs q_{21} and q_{22} need to be measured to split the joint into three four-bar linkage mechanisms. The latter results in three linear equations instead of one nonlinear equation. This submodel also contains two adjustable DOFs $q_{\ell1}$ and $q_{\ell2}$ used for arm length adjustment.

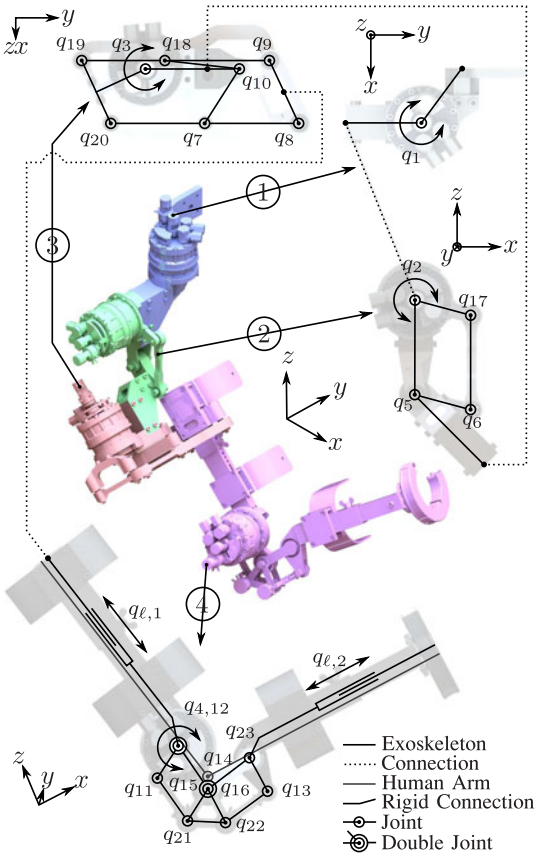

Fig. 7. Actuated DOFs are q_1, q_2, q_3 and q_4. DOFs $q_{\ell 1}$ and $q_{\ell 2}$ are adjustable translational DOFs used for length adjustments of the exoskeleton. All other joints are dependent DOFs ($q_{5\cdots16}$) or constraint DOFs ($q_{17\cdots23}$).

The inertial and dimensional properties of the 18 rigid bodies are extracted from SolidWorks and used for the dynamic modeling in 20-Sim [55]; a modeling and simulation program for mechatronic systems. The rendered SolidWorks model made from .stl files is shown in Fig. 8. A schematic overlay shows the most significant DOFs.

Only the four independent DOFs are relevant for control. The 40 state model (four independent + 16 dependent DOFs with two states per DOF) needs to be reduced to states corresponding to the four independent and two measured DOFs, therefore a state reduction procedure is applied.

B. State Reduction

The 16 dependent joint angles are kinematically related to the four independent actuated and two measured joint angles. The dynamic equation for a multibody system with rigid bodies is

$$M(q)\ddot{q} + C(q,\dot{q})\dot{q} + G(q) = \tau \tag{1}$$

in which $M(q)$ is the orientation dependent mass matrix, $C(q,\dot{q})$ is a matrix containing the Coriolis and centrifugal terms, $G(q)$ is a vector containing the gravity torques, τ the vector of external torques acting on the actuated DOFs and q, $\dot{q}$ and $\ddot{q}$ are, respectively, the vectors of the angles, angular velocities, and angular accelerations of the revolute joints.

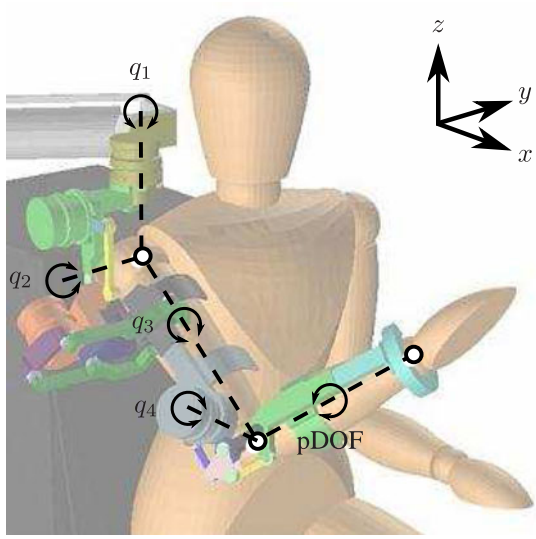

Fig. 8. Model in 20-Sim visualized with .stl files from SolidWorks. The different colors represent the various rigid bodies. The axis of rotation and the shoulder, elbow and wrist joint are represented by the dashed lines and dots, respectively.

The complete kinematic relations are expressed as

$$\begin{aligned} q &= Tq_r \text{ with} \\ q &= [q_1, ..., q_{22}]^T \text{ and} \\ q_r &= [q_1, q_2, q_3, q_4, q_{21}, q_{22}]^T \end{aligned} \tag{2}$$

where the complete state vector q is related to the reduced state vector q_r using the transformation matrix T. The transformation matrix T is a matrix formulation of the following equations:

$$\begin{aligned} q_1 &= q_1 \\ q_2 &= q_5 = q_6 = q_{17} \\ q_3 &= q_7 = q_8 = q_9 = q_{10} = q_{18} = q_{19} = q_{20} \\ q_4 &= q_{14} \\ q_{21} &= q_{11} = q_{12} = q_{15} \text{ and} \\ q_{22} &= q_{13} = q_{16} = q_{23}. \end{aligned} \tag{3}$$

The state reduction begins with the first and second time derivative of (2)

$$\dot{q} = T\dot{q}_r \tag{4}$$

$$\ddot{q} = T\ddot{q}_r \tag{5}$$

which can be substituted in (1) resulting in

$$T^T M(q)T\ddot{q}_r + T^T C(q,\dot{q})T\dot{q}_r + T^T G(q) = T^T\tau \tag{6}$$

which can be rewritten as

$$M_r(q_r)\ddot{q}_r + C_r(q_r,\dot{q}_r)\dot{q}_r + G_r(q_r) = \tau_r \tag{7}$$

with

$$M_r(q_r) = T^T M(q)T \tag{8}$$

$$C_r(q_r,\dot{q}_r) = T^T C(q,\dot{q})T\dot{q}_r \tag{9}$$

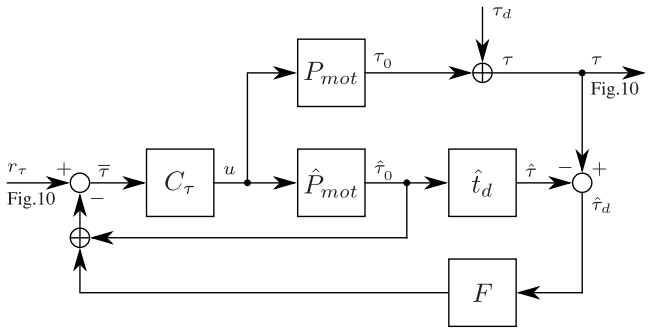

Fig. 9. Torque loop for a single motor contains a lead-lag controller C_τ, the actual motor plant P_{mot}, an estimated motor plant $\hat{P}_{\mathrm{mot}}$, an estimated time delay $\hat{t}_d$ and a filter F. The signals are the reference torque r_τ from the state feedback controller combined with the determined gravity vector (see Fig. 10), the error torque $\overline{\tau}$, the control output u, the undisturbed plant output τ_0, the disturbance torque τ_d, the measured (and generated) torque τ acting on the exoskeleton (see Fig. 10), the nondelayed estimated output $\hat{\tau}_0$, the estimated delayed torque $\hat{\tau}$ and the estimated disturbance torque $\hat{\tau}_d$.

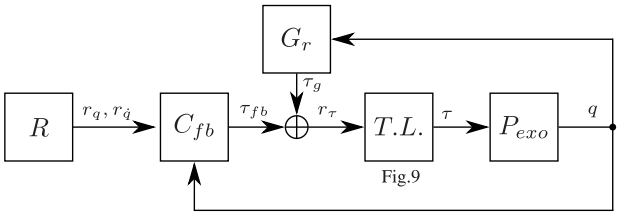

Fig. 10. Impendance control scheme showing the (R)eference generator that calculates the position and velocity reference, the controller C_{fb} containing the state feedback controller [see (13)], the reduced gravity vector G_r, the torque loop $T.L.$ for each motor (see Fig. 9) and the plant P_{exo}. Shown are also the reference signal r_q and its first derivative $r_{\dot{q}}$, the torque vectors from the feedback τ_{fb} controller, the actuator τ (see Fig. 9) and gravity compensator τ_g and the measured positions q. Note that in this figure all lines represent 4-D column vectors representing each actuated joint.

$$G_r(q_r) = T^T G(q) \tag{10}$$

$$\tau_r = T^T \tau. \tag{11}$$

The subscript r refers to the reduced model. Premultiplication with T^T ensures the conservation of energy, keeps a square mass matrix and reduces the number of equations.

IV. Control

A. General Overview

The control algorithm is executed using a xPC-Target (The Mathworks, MA) computer sampling at 1 kHz. The xPC-Target has two national instruments PCI-6229 DAQ cards and one PCI-6602 DAQ card for the data acquisition. The target computer runs the controller. Part of the controller contains the LIMPACTs dynamic equations extracted from 20-Sim (C-code).

The control structure consists of an inner-loop torque (see Fig. 9) and an outer-loop impedance controller (see Fig. 10). The torque controller consists of a lead-lag filter combined with a Smith predictor. Each motor has its own torque controller and all torque controllers are identical. The impedance controller contains the gravitation vector used to compensate for gravitational effects and a state feedback controller. The state feedback controller uses the reference position and velocity in combination with a stiffness and damping matrix to regulating each joint's position and velocity.

B. Joint Torque Control

The hydraulic pump and motor are connected using hoses with a length of 4 m, causing a time delay of approximately 12 ms, which limits performance of the controlled system. A Smith predictor [56] is therefore implemented as it is a dead time compensating controller.

The control structure is shown in Fig. 9. The plant P_{mot} of the motor contains a time delay t_d therefore an estimated plant $\hat{P}_{\mathrm{mot}}$ is incorporated in the control algorithm to estimate a nondelayed response $\hat{\tau}_0$. The estimated response is used to determine the torque error $\overline{\tau}$ to the torque reference r_τ making the controller C_τ more "patient" by creating an immediate response. The estimated response enables the controller gains to be set higher creating a faster controlled system.

The output u from C_τ is used as an input to the real and estimated plant. The torque controller C_τ contains a lead and lag compensator and is formulated as

$$C_\tau(s) = \underbrace{k_i \frac{1+sT_i}{sT_i}}_{\text{Lag}} \cdot \underbrace{k\alpha \frac{1+sT}{1+s\alpha T}}_{\text{Lead}} \tag{12}$$

where k_i is the lag gain and T_i is the lag compensators time constant. The lead compensator is tuned by setting its time constant T, its gain k and the ratio α. The latter is bounded by $0 < \alpha < 1$ to obtain a lead compensator.

To compensate for model inaccuracies and disturbances, the sensor signal τ containing the undisturbed response of the plant τ_0 and the torque disturbance τ_d is also used. A delayed estimated response $\hat{\tau}$ using an estimated time delay $\hat{t}_d$ is then subtracted from the measured torque τ to determine the estimated disturbance torque $\hat{\tau}_d$, which includes the real disturbance and unmodeled responses. This signal is filtered using a 100-Hz second-order Butterworth filter with a relative damping of $\sqrt{2}$. This signal is added to the torque error signal $\overline{\tau}$.

The Smith predictor uses an estimated model of the system. Since the hydraulic system is nonlinear, multiple estimated models were computed using measured system responses to pseudo random binary signals (PRBS) with various amplitudes. Out of this set of estimated models one model was chosen such that the output error is underestimated, leaving the controlled system less aggressive and slightly more dependent on the lead-lag controller than on the model-based Smith predictor.

C. Impedance Controller

Controlling the exoskeleton in its joint space requires the application of stabilizing controllers. Since the exoskeleton is described by nonlinear dynamic equations, linear control theory is not directly applicable unless feedback linearization is applied. Model-based gravity compensation is a specific case of and a first step in feedback linearization. The torques induced by gravity τ_g are compensated for using the reduced gravity

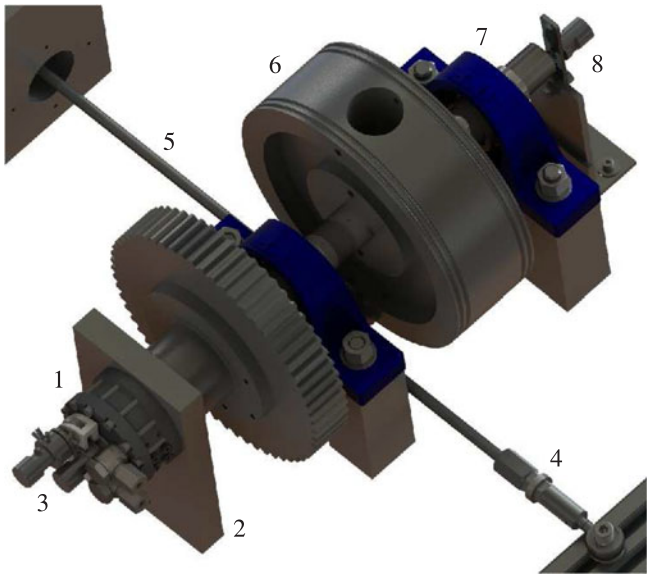

Fig. 11. Experimental setup used to tune the torque and position controller. The hydraulic motor (1) is connected to the base plate (2) which also acts as the housing for the series elastic element. The deformation of the series elastic element can be measured using the encoder (3). Alongside the encoder is a potentiometer and encoder mounted to measure the motor angle. The torque of the motor is measured using the Futek LCM200 force sensor (4) which is pretensioned using a long, low stiffness rod (5). Disconnecting the sensor (4) and rod (5) will enable the motor to rotate the inertia wheel (6) to tune a position controller. The setup is equipped with SKF bearing blocks (7). A redundant encoder (8) is used to measure the load angle.

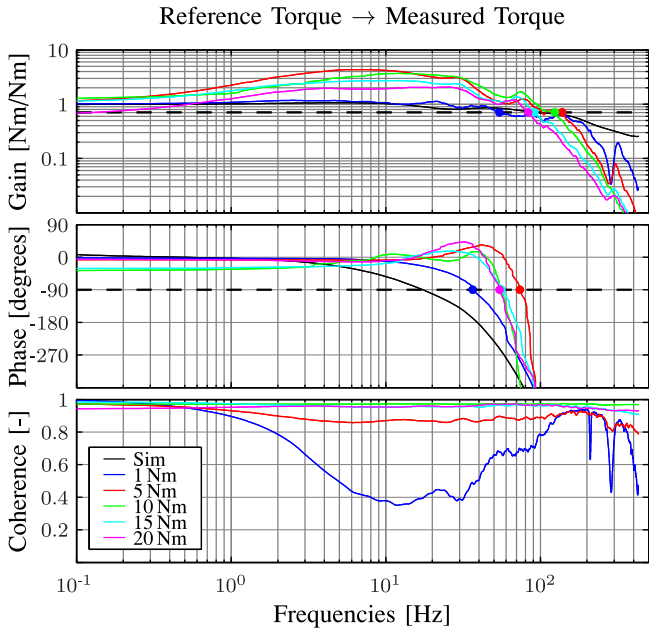

Fig. 12. Frequency measured torque responses to pseudo random binary torque input signals at different amplitudes. The dots either show the crossing with the −3-dB gain line or the −90° phase line for bandwidth determination. The simulated controlled motor is also added with time delay.

vector G_r. A feedback loop is compensating for errors and disturbances [57]. A schematic representation of this control scheme is shown in Fig. 10.

The references for the position r_q and velocity $r_{\dot{q}}$ are computed in the reference generator R. The position and velocity are used by the feedback controller C_{fb}, where the position and velocity errors are calculated using the measured angles

$$\tau_{fb} = K(r_q - q) + D(r_{\dot{q}} - \dot{q}) \tag{13}$$

where K is the virtual stiffness and D the virtual damping matrix, both containing only diagonal terms. The measured signal is differentiated and low pass filtered (10 Hz) to determine the velocity $\dot{q}$.

D. Stability

The complete-controlled LIMPACT needs to be stable. Therefore, both the torque and impedance controller need to be stable to create a completely stable exoskeleton. The torque controller C_τ is tuned using an estimated eighth order motor plant $\hat{P}_{\text{mot}}$. The lag compensator time constant T_i is set at 8 ms to increase the controller gain at frequency below 20 Hz. The lead time constant is set at 69 ms which in combination with a ratio α of 0.15 results in a peak phase lead located at 6 Hz. The combined gain $k_i k$ is set at 60 mv/Nm for an acceptable crossover frequency.

The modeled motor with controller has a phase margin of 114°. The gain margin is infinite since the open loop never reaches a phase of 180°. The maximum feasible gain is limited due to the nonlinearity of the plant, the maximum bandwidth of 300 Hz of the valve and the maximum pressure of 8 MPa. The closed loop transfer function from reference torque to measured torque of the simulated controlled motor is shown in Fig. 12 in Section V including time delay. Note that the controller is tuned using an estimated model of the motor without time delay. The estimated closed loop bandwidth determined at −3 dB using the estimated plant $\hat{P}_{\text{mot}}$ is 56 Hz. The actual bandwidth is determined in Section V.

A system controlled to behave passively is a system which outputs always equal or less energy than has been put into it. Any passive system is stable, and an interconnection of passive systems is also passive. Note that passivity is the property of a (sub)system, for example, a human limb, a robot or an environment, but not a property of a human–robot combination. If all subsystems are passive, than the combinations of those subsystems is also passive. Making the robot a passive system ensures passivity if the human limb acts passive [58]. An additional benefit of passivity is also the inclusion of guaranteed contact stability.

The impedance controller (13) contains a virtual stiffness matrix K and virtual damping matrix D. The controller acts as virtual coupling [59] rendering passive spring and damper elements between the exoskeletons (real) position and a (virtual) reference position. The Z-width is the dynamic range of impedances that can be rendered with a haptic display while maintaining passivity. According to [60], the virtual stiffness cannot be higher than the stiffness of the elastic element in the series elastic motor. Several values for the stiffness and damper matrices have been selected and tested. The tests showed that indeed the value of the stiffness matrix should not exceed the mechanical stiffness. The chosen (positive definite) values for the controller stiffness elements seen in Table IV are set slightly

TABLE III
DETERMINED BANDWIDTHS FOR VARIOUS INPUT AMPLITUDES

Amplitude [Nm]	Bandwidth @ −3 dB [Hz]	Bandwidth @ −90° [Hz]
1	54	37
5	138	74
10	124	56
15	92	56
20	84	54

TABLE IV
CONTROLLER STIFFNESS K AND DAMPING D SETTINGS PER JOINT

Joint #	K [Nm/rd]	D [Nm·s/rd]	Slow [s]	Fast [s]
1	160	5	1	0,75
2	160	5	1	0,5
3	160	5	1	0,4
4	90	1	1	0,25

Slow and fast indicate the cycloid ramp periods.

below the mechanical stiffness as an additional safety factor. The values for the damper elements are set as low as possible for a fast position tracking response.

V. RESULTS

A. Motor Controller

The torque controller for the hydraulic motor is tuned using a custom designed test bench (see Fig. 11). When the motor is connected to the test bench, it can be fixed to restrict any rotation. The torque output of the motor is measured using a Futek LCM200 force sensor.

When the motor is fixated, the torque sensor (i.e., spring stiffness) can be calibrated or the controlled torque response of the motor can be determined. The motor can also be connected to a inertia wheel in the test bench. When the motor is released, the position controller can be tuned.

A PRBS is used to determine the frequency torque response of the torque-controlled hydraulic motor. The frequency content of the torque input signal ranges from 61 mHz to 0.5 kHz and has a flat power density spectrum. The signal is repeated five times to average the Fourier terms, to determine the coherence and to smooth the Bode diagram. Different amplitudes of 1, 5, 10, 15 and 20 Nm are chosen for the PRBS to identify the torque bandwidth of the motor at different amplitudes.

The frequency torque responses to those torque input signals can be found in Fig. 12. The determined torque bandwidths at a gain of -3 dB and phase of -90° are found in Table III. The results in Fig. 12 also show the frequency response of the simulated controlled motor.

The frequency response shows that the gain approaches unity with increasing amplitude, which is reflected by the coherence. The response to a 1-Nm input signal is an exception to this observation and also shows the lowest coherence. The frequency response shows no (unstable) peaks or eigenfrequencies. The 90° and -3-dB bandwidth differ, because the time delay, caused by the hydraulic hoses, causes the -90° line to be reached faster.

B. Simulation

The state feedback position controller is tuned using the 20-Sim model. Four cycloidal reference signals [55] and their first derivatives are used as input signals. A cycloidal signal is used since it smooth, differentiable and has a low jerk motion profile. The values for the controller stiffness and damping are shown in Table IV as well as the cycloids ramp periods. The latter is the time it takes the signal to reach its end value. The slow and fast cycloidal reference signals are shown in Fig. 13 and the configurations corresponding to the reference signals are displayed in Fig. 14. Simulations of the LIMPACT with no arm, with an arm comparable to that of the rescue dummy and with an arm comparable to a person weighing 90 kg is added as supplementary material. A movie containing visual footage of the simulation, experiment, the performance of the minimal impedance with gravity compensation controller and the LIMPACT combined with virtual reality is also added as supplementary material.

The tracking responses show the coupling effects of the controlled system. The gray lines indicate a change in the reference signal which is also the instance the coupling errors occur. A faster response shows more coupling, especially in joint 2. Fig. 13 also shows a static error clearly seen in joint 2 at 41–43 s. The static error is a consequence of choosing a state feedback controller without an integrator and of a disturbance caused by, in this case, joint 3.

The characteristics of the controlled LIMPACT model are also quantified (see Table V). The tracking error decreases with increasing joint number. Overshoot is in the order of 1% or less and a negative overshoot indicates that the reference value is always higher than the measured value. The static error is the tracking error when it reaches its steady-state value. Disturbances in one joint due to movements of another joint are defined as coupling errors. The settling time is determined when the amplitude of the error varies less then 2 mrd. Note that the static error has no effect on the settling time. When the settling time is 0, no oscillations in the error occur. When the settling time is not available (N.A.), the amplitude of the oscillating error is never less than 2 mrd.

C. Tracking Experiments

The slow and fast cycloid reference used in the 20-Sim simulations are also used in the experiments with the LIMPACT. Faster movements are possible, but will not be as smooth as slower movements. As a last experiment the movements are repeated, but now with the arm of a rescue training dummy (Rescue Randy 48 kg) strapped in. The weights of the upper and lower arm are 0.723 and 1.134 kg, respectively.

The tracking responses are shown in Fig. 13 for the empty and loaded LIMPACT. Compared to the simulation results, similar characteristics are shown, i.e., increasing tracking error and coupling effects with a faster reference signal. The tracking error and coupling effects are even more increased when the dummy

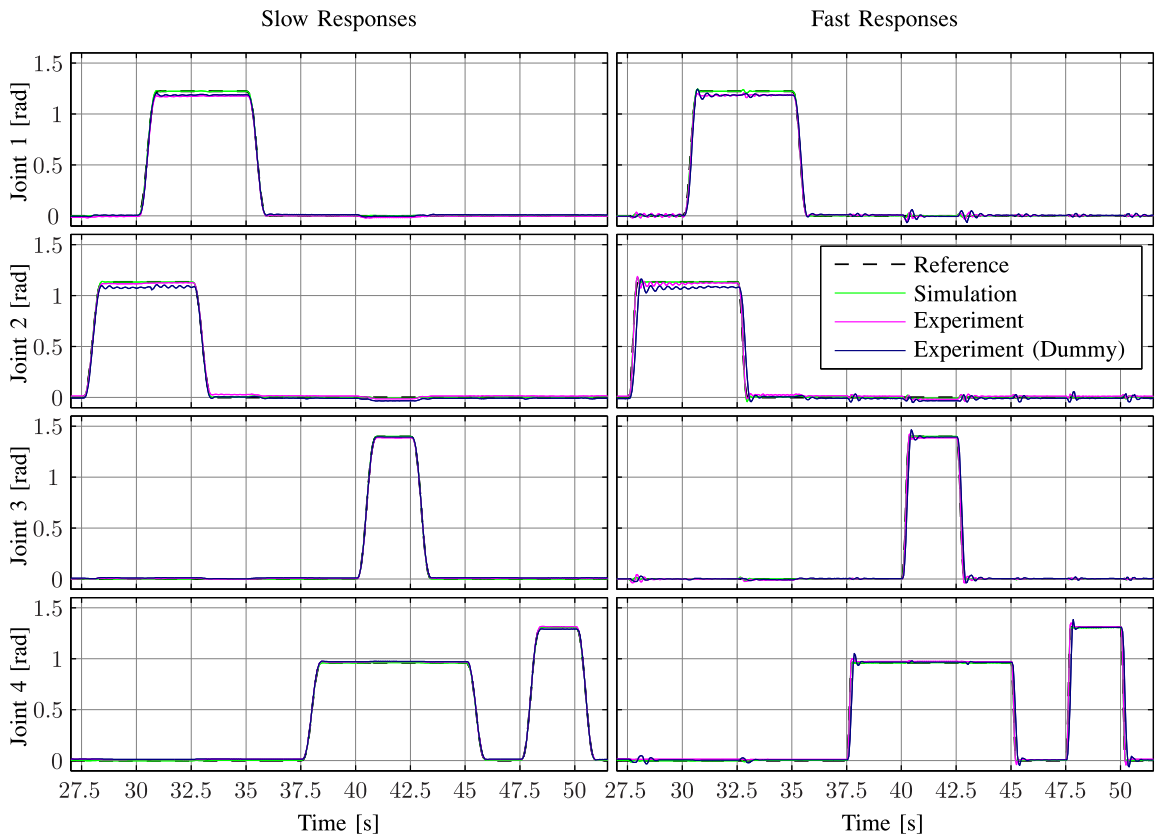

Fig. 13. Tracking of the four experiments showing the responses of a controlled LIMPACT using cycloid reference signals. Slow indicates a slow input signal and fast indicates fast input signal. Dummy indicates that the arm of a rescue dummy was strapped in the LIMPACT. Additional vibrations occur when the dummy is attached since the same controller is used for each experiment, the dummy adds extra inertia and contrary to human limbs, it has no damping in its joints. See Fig. 14 for a graphical representation of the reference movement.

arm is strapped in. Additional vibrations occur when the dummy is attached since the same controller is used for each experiment, the dummy adds extra inertia and unlike a human limb, it has no damping in its joints. Despite the fact that the LIMPACT shows increased oscillatory behavior, the system remains stable.

The quantified characteristics are shown in Table V. The empty LIMPACT has a tracking error with a slow reference as low as 14 mrd which is only increased to 18 mrd when loaded. When moving faster the tracking error can reach up to 89 and 131 mrd, respectively, for the empty and loaded LIMPACT. Overshoot remains below 10% at all times with an average over all value of 2%. The measured static error remains below 40 mrd. Dynamic coupling errors vary in the range of 8 to 79 mrd, which in general, is much lower than the tracking error. Settling times cannot always be properly determined, but can be in the range of 100 to 200 ms as has been demonstrated.

D. Gravity Compensation

The accuracy of the gravity compensation of the LIMPACT is tested by measuring the exoskeleton's weight in various positions using a digital force sensor (Kern HDB 10K10) at the wrist. Measurements are carried out with and without model-based gravity compensation, giving a rough approximation of the accuracy of the reduced gravity vector. The mean and standard deviation of the gravitational forces are 45 ± 6 N without gravity compensation which is reduced to 1 ± 8 N when gravity compensation is activated.

E. Accuracy

The measuring accuracy of the LIMPACT is tested by fixing the endpoint to a linear guidance rail (THK SRS15WN) using a ball joint. The guidance is positioned at various positions and different orientations. Using the LIMPACTs angular sensors and the kinematic model, the endpoint movements are estimated. The measurements are done with the LIMPACT in zero impedance mode and with gravity compensation. The latter combined with the guidance and ball joint results in an experiment where the LIMPACTs mass is not supported. An indication of the accuracy of the LIMPACTs model in combination with its sensors can be determined.

A measure of accuracy is determined by fitting a straight line through the estimated endpoint measurements. Fitting is done using the singular value decomposition method. The fitted line and the estimated endpoint measurements are used to determine the error indicating the measuring accuracy and repeatability of the LIMPACT within its working range. The standard deviation

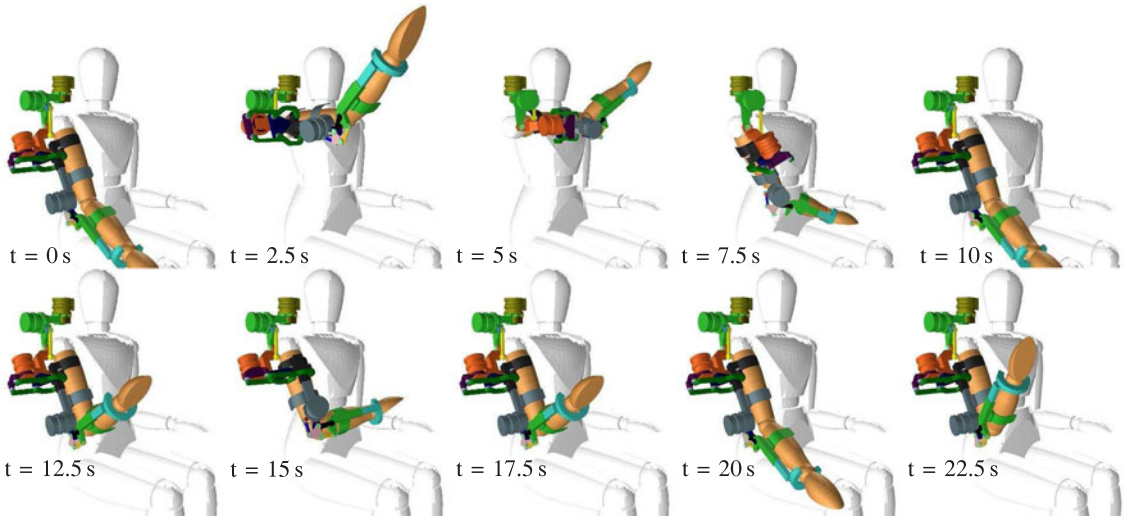

Fig. 14. Graphical representation of the reference movement (see Fig. 13) used in the simulations and experiments.

of the error to the estimated straight line is between 0.7 to 4.3 mm with a mean of 2.4 mm derived from 28 measurements in various orientations.

VI. Discussion

The LIMPACT is designed to be light with powerful motors, to have a short do on/do off (don/doff) time, to be dynamically transparent and safe. According to Table I, most of the (critical) design targets are met. Next to that, the LIMPACT is capable of compensating gravitational forces and accurately measuring positions. Experiments indicate that the LIMPACT can be faster than normal human movements. Using an arm of a rescue dummy during experiments proved that the self-alignment mechanisms perform well and that LIMPACT is able to cope with the extra weight and inertia with minimum performance loss while remaining stable.

To use the exoskeleton for diagnostic purposes not only maximum torque is important, but also torque bandwidth or power [6], [30], [31], [61]. For several exoskeletons the maximum torque, the brand and type of the motor or the maximum velocity are reported, but the torque bandwidth or motor power are hardly reported. The LIMPACT has an amplitude dependent torque bandwidth of 43–102 Hz which is high compared to a torque bandwidth of 40–50 Hz of the X-Arm-2, the highest reported torque bandwidth of an exoskeleton in the literature. This high bandwidth ensures that the LIMPACT can apply torque perturbations with a frequency content of 20 Hz [5], [6] can be created for identification purposes.

The hydraulic actuators of the LIMPACT ensure that these high torques and power can be generated using lightweight actuators. However, this power is generated at a distant locational using a 7.5-kW electric motor connected to a hydraulic pump. This installation is quite expensive (approximately $50 000), has a footprint of 2 m^2 and cannot be placed in hospitals or clinics due to the possibility of oil spills. The system will therefore only be used in a research environment to acquire information on joint reflexes for designing optimal patient specific therapy programs. This information can be used in clinics and hospitals.

An exoskeleton should not impede in the movements of the patient. Tracking of low torques to create a suitable zero-impedance mode is therefore essential. The LIMPACT has a torque sensor resolution of 2 mNm/pulse to measure these low torques. When looked at the torque fidelity of the LIMPACT the high resolution seems somewhat disputable in relation to the torque fidelity. The coherence, a measure for fidelity, drops below 0.4 when a PRBS with an amplitude of 1 Nm is applied (see Fig. 12). However, this drop starts at around 2 Hz which is in the order of the maximum torque control bandwidth of the human limb [38] such that it will not hinder the patient during movements. Since perturbation signals will require higher torque amplitudes at which the coherence approaches unity, this problem will no longer exist.

Designing a light exoskeleton is also a good way to avoid impedance of the natural movements of the patient. The LIMPACT with its mass of 8.0 kg seems rather heavy compared to some exoskeletons [7], [11], [15], [16], [18], [27]–[29]. The lightest of these exoskeletons [29] has a mass of 0.85 kg and is designed for minimal support in rehabilitation. Each DOF can deliver a maximum torque of 8 Nm. The heaviest exoskeleton of this selection [15] has a mass of 6.8 kg which is comparable to the LIMPACT. It can produce a maximum torque of 62 Nm. These exoskeletons may be light enough to enable low-impeded movements, but they are not fast enough for diagnostic experiments. Exoskeletons that are heavier than the LIMPACT [8], [10], [21] are either low torque or do not specify their performance.

The LIMPACT was designed to automatically align the shoulder and elbow joints. Only two of the mentioned exoskeletons [17], [28] also have build-in self-alignment mechanism. However, these exoskeletons only align the shoulder joint and

TABLE V
QUANTIFIED PERFORMANCE OF THE CONTROLLED LIMPACT AT SLOW AND FAST MOVEMENTS

			Joint 1			Joint 2			Joint 3			Joint 4		
			Sim	Exp.	Exp. D.	Sim	Exp.	Exp. D.	Sim	Exp.	Exp. D.	Sim	Exp.	Exp. D.
Tracking error	[mrd]	Slow	22	50	68	10	20	58	3	20	18	3	14	28
Overshoot	[%]		0	−3	−9	0	−2	−2	0	−1	0	0	1	2
Static error	[mrd]		0	46	35	2	15	N.A.	2	12	10	3	12	18
Settling time	[ms]		131	N.A.	N.A.	0	413	N.A.	0	0	0	0	123	166
Coupling error	[mrd]		4	23	16	9	15	37	4	8	6	4	6	4
From Joint	[-]		3	3	3	3	3	3	2	2	1	1	2	3
Tracking error	[mrd]	Fast	33	77	109	56	89	131	20	69	70	22	96	87
Overshoot	[%]		1	−10	5	4	5	4	0	3	6	0	4	10
Static error	[mrd]		2	N.A.	39	2	N.A.	N.A.	2	11	8	3	12	7
Settling time	[ms]		50	N.A.	N.A.	290	N.A.	N.A.	30	398	1240	15	650	900
Coupling error	[mrd]		24	64	73	25	43	79	20	43	28	15	9	33
From Joint	[-]		3	3	3	3	3	4	2	1	2	2	3	2

require a controller for the aligning movements. Others are working on self-aligning shoulder mechanisms [62]–[64], but have not yet shown a working prototype. The LIMPACT is the only exoskeleton known to the authors that can automatically align the shoulder and elbow without a controller and motor. An additional advantage of the chosen implementation is that it passively balances the system.

The LIMPACT is suitable for use in neurorehabilitation. Combining the gravity compensation, torque sensor resolution and torque bandwidth of the LIMPACT results in an exoskeleton that feels lightweight and moves smoothly. Stroke patients often already have difficulties in moving their affected limb and the LIMPACT should not impede the movements they can still make. Compared to current rehabilitation upper limb exoskeletons [11], [15]–[21], [23]–[25], [27], [28] the LIMPACT has a small amount of actuated DOFs and average ROM. However, the number of DOFs and ROM are sufficient to train in a large number of ADL tasks [15].

Based on the experimental results, the LIMPACT seems suitable for diagnostic measurements as for instance done by McPhersen *et al.* [4]. Here, the relationship between the flexion synergy and stretch reflexes in chronic hemiparetic stroke patients is determined. To elicit reflexes, the elbow was perturbed with velocities up to 4.7 rd/s with increasing shoulder abduction while measuring interaction forces. The LIMPACT has proven to produce velocities up to 6.5 rd/s with test dummy strapped in, however interaction forces are not measured directly since part of the exoskeleton is between the torque sensor and the human arm. Another diagnostic measurement that can be performed by the LIMPACT is determining the work area at various limb load levels in stroke patients [65]–[67]. Note that in the latter experiments the interaction and gravity forces are measured directly in a single DOF setup. In the LIMPACT as in general in other exoskeletons, the gravity and interaction forces are measured indirectly in a multi-DOF setup using the exoskeleton's model.

The series elastic motor choice inherently affect position tracking performance. For better diagnostic measurements on stroke patients, the LIMPACT's position tracking performance has to be improved with respect to tracking errors and speed [6], [30], [31], [61]. One way to achieve this, is to make the elastic element stiffer [53]. Another way is to improve the performance of the torque controller. Note that the current tracking experiment is the worst case. The amplitudes used in the experiments demonstrate the reachable working area of the LIMPACT and are therefore quite large. Reducing the amplitude will reduce coupling effects which will have a positive effect on tracking errors and possibly settling times. This can create the opportunity to increase speeds while still having an acceptable performance.

Currently, the hydraulic motor is torque controlled using a linear controller. The controlled hydraulic system is still a nonlinear system, which is shown by the differing frequency responses at various input amplitudes. Model-based control can linearize the system and improve (torque tracking) performance for the inner loop control [53]. A model-based controller for our hydraulic motor is under development.

The observed static errors occur due to perturbations from coupling, in combination with a state feedback controller containing only stiffness and damping. Improving the LIMPACT's outer loop controller by implementing the model's Coriolis and centrifugal matrix, will complete the model-based linearization. Premultiplying the control signal with the mass matrix will decouple the system. As a last step, the reduced mass matrix can be multiplied with the reference acceleration to determine a feedforward torque. These improvements will enhance performance and reduce control effort. Implementation of this controller and testing its zero impedance [68] is also planned as future study.

ACKNOWLEDGMENT

The authors would like to thank W. Abbas, S. M. Behrens, A. Q. L. Keemink and N. A. Melikian for their technical advice and support during the build of and experimenting with the LIMPACT.

REFERENCES

[1] J. Mackay, G. Mensah, S. Mendis, and K. Greenlund, *The Atlas of Heart Disease and Stroke.* Geneva, Switzerland: World Health Org., 2004.
[2] E. J. Perreault, R. F. Kirsch, and P. E. Crago, "Voluntary control of static endpoint stiffness during force regulation tasks," *J. Neurophysiol.*, vol. 87, no. 6, pp. 2808–2816, 2002.
[3] G. Lewis, C. MacKinnon, R. Trumbower, and E. Perreault, "Co-contraction modifies the stretch reflex elicited in muscles shortened by a joint perturbation," *Exp. Brain Res.*, vol. 207, no. 1–2, pp. 39–48, 2010.

[4] J. McPherson, A. H. A. Stienen, J. Drogos, and J. P. A. Dewald, "The relationship between the flexion synergy and stretch reflexes in individuals with chronic hemiparetic stroke," in *Proc. IEEE Int. Conf. Rehabil. Robot.*, 2011, pp. 1–7.

[5] F. C. van der Helm, A. C. Schouten, E. de Vlugt, and G. G. Brouwn, "Identification of intrinsic and reflexive components of human arm dynamics during postural control," *J. Neurosci. Methods*, vol. 119, no. 1, pp. 1–14, 2002.

[6] E. de Vlugt, A. C. Schouten, and F. C. van der Helm, "Quantification of intrinsic and reflexive properties during multijoint arm posture," *J. Neurosci. Methods*, vol. 155, no. 2, pp. 328–349, 2006.

[7] A. Schiele and G. Hirzinger, "A new generation of ergonomic exoskeletons—The high-performance x-arm-2 for space robotics telepresence," in *Proc. IEEE Int. Conf. Intell. Robots Syst.*, Sep. 2011, pp. 2158–2165.

[8] H. Kazerooni, "The human power amplifier technology at the university of california, berkeley," *Robot. Auton. Syst.*, vol. 19, no. 2, pp. 179–187, 1996.

[9] E. Yeates. (2012). Utah-built robot safeguards the workplace [Online]. Available: http://www.ksl.com/?nid=148&sid=17654421&autostart=y

[10] A. Frisoli, F. Salsedo, M. Bergamasco, B. Rossi, and M. C. Carboncini, "A force-feedback exoskeleton for upper-limb rehabilitation in virtual reality," *Appl. Bionics Biomech.*, vol. 6, no. 2, pp. 115–126, 2009.

[11] P. Letier, M. Avraam, S. Veillerette, M. Horodinca, M. De Bartolomei, A. Schiele, and A. Preumont, "Sam : A 7-dof portable arm exoskeleton with local joint control," in *Proc. IEEE Int. Conf. Intell. Robots Syst.*, Sep. 2008, pp. 3501–3506.

[12] M. Guidali, A. Duschau-Wicke, S. Broggi, V. Klamroth-Marganska, T. Nef, and R. Riener, "A robotic system to train activities of daily living in a virtual environment," *Med. Biol. Eng. Comput.*, vol. 49, no. 10, pp. 1213–1223, 2011.

[13] S. E. Fasoli, H. I. Krebs, J. Stein, W. R. Frontera, and N. Hogan, "Effects of robotic therapy on motor impairment and recovery in chronic stroke," *Archives Phys. Med. Rehabil.*, vol. 84, no. 4, pp. 477–482, 2003.

[14] P. Garrec, J. Friconneau, Y. Masson, and Y. Perrot, "Able, an innovative transparent exoskeleton for the upper-limb," in *Proc. IEEE Int. Conf. Intell. Robots Syst.*, 2008, pp. 1483–1488.

[15] J. Perry, J. Rosen, and S. Burns, "Upper-limb powered exoskeleton design," *IEEE Trans. Mechatron.*, vol. 12, no. 4, pp. 408–417, Aug. 2007.

[16] Y. Mao and S. Agrawal, "Design of a cable-driven arm exoskeleton (carex) for neural rehabilitation," *IEEE Trans. Robot.*, vol. 28, no. 4, pp. 922–931, Aug. 2012.

[17] H. Park, Y. Ren, and L. Zhang, "Intelliarm: An exoskeleton for diagnosis and treatment of patients with neurological impairments," in *Proc. 2nd Biennial IEEE Int. Conf. Biomed. Robot. Biomechatron.*, 2008, pp. 109–114.

[18] A. Gupta and M. O'Malley, "Design of a haptic arm exoskeleton for training and rehabilitation," *IEEE Trans. Mechatron.*, vol. 11, no. 3, pp. 280–289, Jun. 2006.

[19] M. Rahman, T. Kittel-Ouimet, M. Saad, J. Kenn, and P. Archambault, "Development and control of a robotic exoskeleton for shoulder, elbow and forearm movement assistance," *Appl. Bionics Biomech.*, vol. 9, no. 3, pp. 275–292, 2012.

[20] S. Ball, I. Brown, and S. Scott, "Medarm: A rehabilitation robot with 5dof at the shoulder complex," in *Proc. IEEE Int. Conf. Adv. Intell. Mechatron.,* 2007, pp. 1–6.

[21] C. Carignan, J. Tang, and S. Roderick, "Development of an exoskeleton haptic interface for virtual task training," in *Proc. IEEE Int. Conf. Intell. Robots Syst.*, Oct. 2009, pp. 3697–3702.

[22] C. Carignan, M. Liszka, and S. Roderick, "Design of an arm exoskeleton with scapula motion for shoulder rehabilitation," in *Proc. 12th Int. Conf. Adv. Robot.*, 2005, pp. 524–531.

[23] D. Caldwell, N. Tsagarakis, S. Kousidou, N. Costa, and I. Sarakoglou, "Soft" exoskeletons for upper and lower body rehabilitation—Design, control and testing," *Int. J. Humanoid Robot.*, vol. 4, no. 3, pp. 549–573, 2007.

[24] W. Chen, C. Xiong, R. Sun, and X. Huang, "A 10-degree of freedom exoskeleton rehabilitation robot with ergonomic shoulder actuation mechanism," *Int. J. Humanoid Robot.*, vol. 8, no. 1, pp. 47–71, 2011.

[25] R. Sanchez, Jr., E. Wolbrecht, R. Smith, J. Liu, S. Rao, S. Cramer, T. Rahman, J. Bobrow, and D. Reinkensmeyer, "A pneumatic robot for re-training arm movement after stroke: Rationale and mechanical design," in *Proc. 9th Int. Conf. Rehabil. Robot.*, 2005, pp. 500–504.

[26] S. Balasubramanian and J. He, "Adaptive control of a wearable exoskeleton for upper-extremity neurorehabilitation," *Appl. Bionics Biomech.*, vol. 9, no. 1, pp. 99–115, 2012.

[27] S. Kousidou, N. Tsagarakis, D. Caldwell, and C. Smith, "Assistive exoskeleton for task based physiotherapy in 3-dimensional space," in *Proc. 1st IEEE Int. Conf. Biomed. Robot. Biomechatron.*, 2006, pp. 266–271.

[28] R. Gopura, K. Kiguchi, and Y. Yi, "Sueful-7: A 7dof upper-limb exoskeleton robot with muscle-model-oriented emg-based control," in *Proc. IEEE Int. Conf. Intell. Robots Syst.*, 2009, pp. 1126–1131.

[29] E. Rocon, J. Belda-Lois, A. Ruiz, M. Manto, J. Moreno, and J. Pons, "Design and validation of a rehabilitation robotic exoskeleton for tremor assessment and suppression," *IEEE Trans. Neural Syst. Rehabil. Eng.*, vol. 15, no. 3, pp. 367–378, Sep. 2007.

[30] A. Schouten, E. de Vlugt, J. van Hilten, and F. van der Helm, "Quantifying proprioceptive reflexes during position control of the human arm," *IEEE Trans. Biomed. Eng.*, vol. 55, no. 1, pp. 311–321, Jan. 2008.

[31] C. Patten, E. Condliffe, C. Dairaghi, and P. Lum, "Concurrent neuromechanical and functional gains following upper-extremity power training post-stroke," *J. NeuroEng. Rehabil.*, vol. 10, pp. 1–19, 2013.

[32] D. M. Wolpert and R. J. Flanagan, "Q & A: Robotics as a tool to understand the brain," *BMC Biol.*, vol. 8, no. 1, pp. 1–4, 2010.

[33] R. Trumbower, V. Ravichandran, M. Krutky, and E. Perreault, "Altered multijoint reflex coordination is indicative of motor impairment level following stroke," in *Proc. 30th Annu. Int. Eng. Med. Biol. Soc.*, 2008, pp. 3558–3561.

[34] T. Nef and R. Riener, "Shoulder actuation mechanisms for arm rehabilitation exoskeletons," in *Proc. 2nd IEEE Int. Conf. Biomed. Robot. Biomechatron.*, 2008, pp. 862–868.

[35] A. Schiele, "An explicit model to predict and interpret constraint force creation in phri with exoskeletons," in *Proc. IEEE Int. Conf. Robot. Autom.*, 2008, pp. 1324–1330.

[36] A. Stienen, E. E. G. Hekman, F. Van der Helm, G. Prange, M. J. A. Jannink, A. M. M. Aalsma, and H. van der Kooij, "Dampace: Dynamic force-coordination trainer for the upper extremities," in *Proc. IEEE 10th Int. Conf. Rehabil. Robot.*, 2007, pp. 820–826.

[37] A. Stienen, E. Hekman, G. Prange, M. Jannink, A. Aalsma, F. van der Helm, and H. van der Kooij, "Dampace: Design of an exoskeleton for force-coordination training in upper-extremity rehabilitation," *ASME J. Med. Dev.*, vol. 3, no. 3, pp. 1–10, 2009.

[38] T. Brooks, "Telerobotic response requirements," in *Proc. IEEE Int. Conf. Syst., Man, Cybern.*, Nov. 1990, pp. 113–120.

[39] H. Kazerooni, "Human-robot interaction via the transfer of power and information signals," *IEEE Trans. Syst., Man, Cybern.*, vol. 20, no. 2, pp. 450–463, Mar./Apr. 1990.

[40] J. Rosen, J. Perry, N. Manning, S. Burns, and B. Hannaford, "The human arm kinematics and dynamics during daily activities—Toward a 7 dof upper limb powered exoskeleton," in *Proc. 12th Int. Conf. Adv. Robot.*, Jul. 2005, pp. 532–539.

[41] Delft University of Technology. (May 2013). Dined: Anthopometric database [Online]. Available: http://http://dined.io.tudelft.nl/ergonomics/

[42] J. Herder, *Energy-Free Systems: Theory, Conception and Design of Statically Balanced Spring Mechanisms*. Delft Univ. Technol. 2001.

[43] A. Stienen, E. Hekman, F. van der Helm, and H. van der Kooij, "Self-aligning exoskeleton axes through decoupling of joint rotations and translations," *IEEE Trans. Robot.*, vol. 25, no. 3, pp. 628–633, Jun. 2009.

[44] U. Onen, F. Botsali, M. Kalyoncu, M. Tinkir, N. Yilmaz, and Y. Sahin, "Design and actuator selection of a lower extremity exoskeleton," *IEEE Trans. Mechatron.*, vol. 19, no. 2, pp. 623–632, Apr. 2014.

[45] H. Olsson, K. J. strm, M. Gfvert, C. C. D. Wit, and P. Lischinsky, "Friction models and friction compensation," *Eur. J. Control*, vol. 4, pp. 176–195, 1998.

[46] K. Ohnishi, M. Shibata, and T. Murakami, "Motion control for advanced mechatronics," *IEEE Trans. Mechatron.*, vol. 1, no. 1, pp. 56–67, Mar. 1996.

[47] C. C. de Wit and P. Lischinsky, "Adaptive friction compensation with partially known dynamic friction model," *Int. J. Adaptive Control Signal Process.*, vol. 11, no. 1, pp. 65–80, 1997.

[48] A. Albu-Schäffer, C. Ott, and G. Hirzinger, "A passivity based cartesian impedance controller for flexible joint robots—Part ii: Full state feedback, impedance design and experiments," in *Proc. IEEE Int. Conf. Robot. Autom.*, Apr. 2004, pp. 2666–2672.

[49] A. Albu-Schäffer, C. Ott, and G. Hirzinger, "A unified passivity-based control framework for position, torque and impedance control of flexible joint robots," *Int. J. Robot. Res.*, vol. 26, no. 1, pp. 23–39, 2007.

[50] C. Ott, A. Albu-Schaffer, A. Kugi, S. Stamigioli, and G. Hirzinger, "A passivity based cartesian impedance controller for flexible joint robots—Part I: Torque feedback and gravity compensation," in *Proc. IEEE Int. Conf. Robot. Autom.*, Apr. 2004, pp. 2659–2665.

[51] J. E. Huber, N. A. Fleck, and M. F. Ashby, "The selection of mechanical actuators based on performance indices," *Proc. Roy. Soc. London, Series A: Math., Phys. Eng. Sci.*, vol. 453, no. 1965, pp. 2185–2205, 1997.
[52] A. Stienen, E. Hekman, H. Ter Braak, A. Aalsma, F. van der Helm, and H. van der Kooij, "Design of a rotational hydro-elastic actuator for an active upper-extremity rehabilitation exoskeleton," in *Proc. IEEE Int. Conf. Biomed. Robot. Biomechatron.*, 2008, pp. 881–888.
[53] A. Otten, W. van Vuuren, A. Stienen, E. van Asseldonk, A. Schouten, and H. van der Kooij, "Position and torque tracking: Series elastic actuation versus model-based-controlled hydraulic actuation," in *Proc. IEEE Int. Conf. Rehabil. Robot.*, 2011, pp. 1–6.
[54] J. Pratt, B. Krupp, and C. Morse, "Series elastic actuators for high fidelity force control," *Ind. Robot: Int. J.*, vol. 29, no. 3, pp. 234–241, 2002.
[55] C. Kleijn, M. Groothuis, and H. Differ, *Reference Manual 20-Sim 4.3*. Enschede, The Netherlands: Controllab Products B.V., 2012.
[56] A. Ingimundarson and T. Hägglund, "Robust tuning procedures of dead-time compensating controllers," *Control Eng. Practice*, vol. 9, no. 11, pp. 1195–1208, 2001.
[57] C. An, C. Atkeson, J. Griffiths, and J. Hollerbach, "Experimental evaluation of feedforward and computed torque control," *IEEE Trans. Robot. Autom.*, vol. 5, no. 3, pp. 368–373, Jun. 1989.
[58] J. E. Colgate, "The control of dynamically interacting systems," Ph.D. dissertation, Dept. Mech. Eng., Massachusetts Inst. Technol., Cambridge, MA, USA, 1988.
[59] R. J. Adams and B. Hannaford, "A two-port framework for the design of unconditionally stable haptic interfaces," in *Proc. IEEE Int. Conf. Intell. Robots Syst.*, 1998, pp. 1254–1259.
[60] H. Vallery, J. Veneman, E. Van Asseldonk, R. Ekkelenkamp, M. Buss, and H. Van Der Kooij, "Compliant actuation of rehabilitation robots," *IEEE Robot. Autom. Mag.*, vol. 15, no. 3, pp. 60–69, Sep. 2008.
[61] A. Schouten, T. Boonstra, F. Nieuwenhuis, S. Campfens, and H. van der Kooij, "A bilateral ankle manipulator to investigate human balance control," *IEEE Trans. Neural Syst. Rehabil. Eng.*, vol. 19, no. 6, pp. 660–669, Dec. 2011.
[62] M. Ergin and V. Patoglu, "Assiston-se: A self-aligning shoulder-elbow exoskeleton," in *Proc. IEEE Int. Conf. Robot. Autom.*, May 2012, pp. 2479–2485.
[63] D. Galinski, J. Sapin, and B. Dehez, "Optimal design of an alignment-free two-dof rehabilitation robot for the shoulder complex," in *Proc. IEEE Int. Conf. Rehabil. Robot.*, Jun. 2013, pp. 1–7.
[64] Y. Jung and J. Bae, "Kinematic analysis of a 5-dof upper-limb exoskeleton with a tilted and vertically translating shoulder joint," in *Proc. IEEE/ASME Int. Conf. Adv. Intell. Mechatronics*, Jul. 2013, pp. 1643–1648.
[65] M. D. Ellis, T. Sukal, T. DeMott, and J. P. A. Dewald, "Augmenting clinical evaluation of hemiparetic arm movement with a laboratory-based quantitative measurement of kinematics as a function of limb loading," *Neurorehabil. Neural Repair*, vol. 22, no. 4, pp. 321–329, 2008.
[66] T. Sukal, M. Ellis, and J. Dewald, "Shoulder abduction-induced reductions in reaching work area following hemiparetic stroke: Neuroscientific implications," *Exp. Brain Res.*, vol. 183, no. 2, pp. 215–223, 2007.
[67] R. F. Beer, J. P. Dewald, and W. Z. Rymer, "Deficits in the coordination of multijoint arm movements in patients with hemiparesis: Evidence for disturbed control of limb dynamics," *Exp. Brain Res.*, vol. 131, no. 3, pp. 305–319, 2000.
[68] B. Ugurlu, M. Nishimura, K. Hyodo, M. Kawanishi, and T. Narikiyo, "A framework for sensorless torque estimation and control in wearable exoskeletons," in *Proc. 12th IEEE Int. Workshop Adv. Motion Control*, Mar. 2012, pp. 1–7.

Alexander Otten received the B.Sc. degree in mechanical engineering from the Inholland University of Applied Sciences, Alkmaar, The Netherlands, in 2005, and the M.Sc. degree in mechanical engineering from the University of Twente, Enschede, The Netherlands, in 2009.

He has worked on the modeling and design of machinery which can process a.o. diary, cryogenic liquids or gases and composites. Furthermore, he has modeled, designed and optimized several MEMS actuators. He is currently working as a Factory Engineer responsible for production automation at Handicare Stairlifts, Heerhugowaard, The Netherlands.

Carsten Voort received the B.S. degree in mechanical engineering from the University of Twente, Enschede, The Netherlands, in 2009, and the M.Sc. degree in biomechanical engineering from the University of Twente in 2011.

He is currently working on a state of the art rehabilitation robot for assistance in balance and walking. His main responsibilities in this project include mechatronic and software design, system assembly and the real-time software implementation. His research interests include the field of rehabilitation robotics, wearable exoskeletons, mechatronic design and control, electronics, microcontrollers and programming.

Arno Stienen received the M.Sc. degree in mechanical engineering from the Delft University of Technology, Delft, The Netherlands, in 2003, and the Ph.D. degree in rehabilitation robotics from the University of Twente, Enschede, The Netherlands, in 2009.

His work relates to the advancement of biomechatronics and human–robot interaction, for instance, for automated therapy after stroke or the support of lifting heavy objects for industrial users. He currently holds the positions of Assistant Professor at the University of Twente and Northwestern University, Chicago, IL, USA. He is also the Program Director of the Professional Doctorate in Engineering in Robotics, University of Twente.

Ronald Aarts received the M.S. and Ph.D. degrees in applied physics from the Eindhoven University of Technology, Eindhoven, The Netherlands, in 1988 and 1993, respectively.

He is currently an Associate Professor at the Department of Mechanical Automation and Control, University of Twente, Enschede, The Netherlands. His research and teaching interests include systems and control, mechatronics, (flexible) multibody dynamics and system identification.

Edwin van Asseldonk received the Ph.D. degree in 2008.

He is currently an Assistant Professor at the Department of Biomechanical Engineering, University of Twente, Enschede, The Netherlands. His main interests include human motor control and adaptation in the lower extremities, brain plasticity and rehabilitation robotics. He is an Investigator on several Dutch and European Union projects on rehabilitation robotics and noninvasive brain stimulation. He has published more than 50 papers and conference proceedings in the area of balance control during stance and walking, motor adaptation, lower limb rehabilitation robotics.

Herman van der Kooij received the Ph.D. degree (*cum laude*) in 2000.

He is currently a Professor in biomechatronics and rehabilitation technology at the Department of Biomechanical Engineering, University of Twente, Enschede, The Netherlands, and the Delft University of Technology, Delft, The Netherlands. His expertise and interests include the field of human motor control, adaptation, and learning, rehabilitation robots, diagnostic, and assistive robotics, virtual reality, rehabilitation medicine, and neuro computational modeling. He has published more than 100 publications in the area of biomechatronics and human motor control.

Prof. van der Kooij is an Associate Editor of IEEE TRANSACTIONS ON BIOMEDICAL ENGINEERING. He is a Member of IEEE EMBS Technical Committee of Biorobotics, and was a member of several scientific program committees in the field of rehabilitation robotics, bio robotics, and assistive devices.